LAWRENCE
LIVERMORE
NATIONAL
LABORATORY

LLNL-JRNL-789697

Role of manganese on accelerating the oxidation of Pb(II) carbonate solids to Pb(IV) oxide at drinking water conditions

W. Pan, C. Pan, Y. Bae, D. Giammar

September 13, 2019

Environmental Science & Technology

Disclaimer

The role of manganese in accelerating the oxidation of Pb(II) carbonate solids to Pb(IV) oxide at drinking water conditions

Weiyi Pan[†], Chao Pan[†‡*], Yeunook Bae[†], and Daniel Giammar[†]

[†]Department of Energy, Environmental & Chemical Engineering, Washington University in St. Louis, Missouri 63130, United States.

[‡]Physical & Life Sciences, Lawrence Livermore National Laboratory, 7000 East Avenue, Livermore, California 94550, United States.

*Corresponding Author

*Phone: (314) 608-8987; e-mail: pan10@llnl.gov (C. Pan)

IM release number: LLNL-JRNL-775405

ABSTRACT

Pb(II) carbonate solids are corrosion products that form on the inner surfaces of lead service lines (LSLs) and can be oxidized by free chlorine to form Pb(IV) oxide (PbO_2). The formation of PbO_2 can maintain low dissolved lead concentrations in drinking water, but PbO_2 can dissolve if a free chlorine residual is not maintained. Experiments demonstrated that the oxidation of Pb(II) carbonate by free chlorine was faster with manganese (Mn). Without Mn(II), the oxidation of Pb(II) carbonate was an autocatalytic process. With Mn(II), the overall oxidation rate was two orders of magnitude faster than without Mn(II). X-ray diffraction and free chlorine consumption profiles indicated that δ-MnO_2 was formed within several minutes of the reaction of Mn(II) with free chlorine, and δ-MnO_2 catalyzed the oxidation of Pb(II) carbonate by free chlorine. Free chlorine consumption profiles for Pb(II) carbonate with and without Mn(II) were interpreted based on the kinetics and stoichiometry of the underlying chemical reactions. These findings highlight the importance of Mn in accelerating the formation of PbO_2 in water with Pb(II) carbonate solids and free chlorine, and it may help explain why PbO_2 is observed on LSLs of some but not all water systems that use free chlorine.

Key words: Manganese, Pb(II) carbonate, Pb(IV) oxide, catalytic oxidation, drinking water

Graphical Abstract

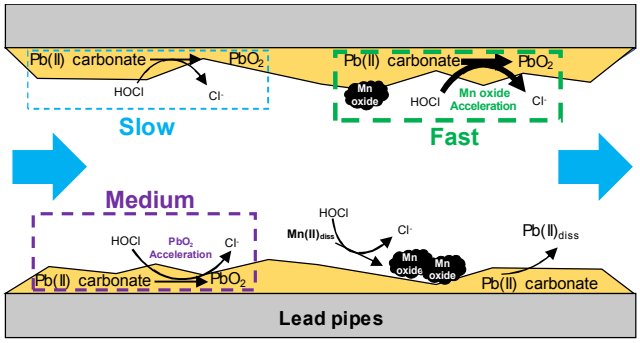

Introduction

Ingestion of lead-contaminated drinking water is one of the major pathways for human exposure to lead.[1–3] Lead service lines (LSLs) and premise plumbing are the largest sources of lead to drinking water.[2] In the United States, the Lead Copper Rule has an action level of 0.015 mg/L lead for the 90th percentile of specific homes' 1-L first draw samples of tap water that triggers additional actions if it is not met.[4] Although the 1986 Safe Drinking Water Act Amendments banned lead pipes, fittings, fixtures, solder and flux, millions of partial or whole lead service lines are still present in the United States.[3,5,6]

Lead concentrations in drinking water are controlled by the solubility of lead corrosion products that form in lead pipes and premise plumbing.[7–12] These corrosion products include Pb(II) carbonate, oxide, and phosphate solids as well as Pb(IV) oxide (PbO_2).[9,10,13,14] Previous studies have shown that the oxidation of Pb(II) carbonate, including cerussite ($PbCO_3$) and hydrocerussite ($Pb_3(CO_3)_2(OH)_2$), by free chlorine will lead to the formation of lead(IV) oxide.[8,15,16] Liu et al.[16] reported an autocatalytic reaction during Pb(II) carbonate oxidation by chlorine. Wang et al.[8] found that the identity and rate of formation of the PbO_2 phases produced from reaction of various Pb(II) species with free chlorine were affected by the initial solid or dissolved Pb(II) species, dissolved inorganic carbon (DIC), pH, and free chlorine concentration.[17] PbO_2 has two phases, scrutinyite (α-PbO_2) and plattnerite (β-PbO_2), both of which have a low solubility compared with Pb(II) corrosion products. Triantafyllidou et al.[18] reported that lead release from lead pipes coated with Pb(IV) oxides was consistently much lower than from pipes coated with Pb(II)-containing solids and hence concluded that formation of PbO_2 in LSLs could be an effective lead corrosion control strategy.[18] The depletion of free chlorine, lower oxidation reduction potential (ORP) disinfectants (such as monochloramine), and the presence of reductants (natural organic matter, Br^-, I^-, Fe(II),

and Mn(II), etc.) may lead to the dissolution of PbO_2.[19–25] The increases in lead concentrations in Washington, DC tap water that begins in late 2000 were triggered by a change in disinfectant from higher ORP free chlorine to lower ORP monochloramine.[26] While PbO_2 has been observed on many LSLs from water systems that use free chlorine,[10,12,14,18] PbO_2 has not always been observed in the scales of LSLs for such systems.[10,12,18] The limited range of conditions over which PbO_2 is stable may limit its observation. While PbO_2 can be formed by reaction with free chlorine, it is only stable when a free chlorine residual is present and PbO_2 can be reduced by reductants such as natural organic matter, I^-, Br^-, Fe(II), Mn(II), and even water (Figure 1) when free chlorine is depleted.[19,21–25]

Manganese accumulation has been reported in different water distribution systems.[11,27–30] The accumulated Mn in water distribution systems is generated from oxidation of soluble Mn(II) by free chlorine, oxygen, and other oxidants to form insoluble Mn(III) and Mn(IV) solids.[27,28,31] In addition, the activity of manganese depositing microbes can also give rise to the formation of manganese oxides in drinking water networks.[27,32–35] Gerke et al.[33] reported that birnessite (Mn(III) and Mn(IV)), hollandite (Mn(II) and Mn(IV)), and braunite (Mn(II) and Mn(IV)) were the main Mn oxides/oxyhydroxide in water distribution systems. The interactions between Pb and Mn may represent a sink or source for lead and Mn in drinking water, and previous studies have investigated the adsorption of Pb(II) on Mn(III, IV) oxides[36–38] as well as the oxidation of Mn(II) by lead(IV) oxide.[25,39] Matocha et al.[39] revealed that Pb(II) was adsorbed as inner-sphere complexes on both birnessite and manganite, and they found no evidence of Pb(II) oxidation by birnessite and manganite based on X-ray absorption fine structure (XAFS) spectra. Shi and Stone[25] studied the redox reaction between PbO_2 and Mn(II), and they found that Mn(II) could be oxidized to Mn(III)

or Mn(IV) (hydr)oxides (MnOOH and σ-MnO_2) by PbO_2. This result is consistent with Figure 1, which illustrates that PbO_2 is a stronger oxidant than Mn(IV) oxide.[25]

Although recent investigations have examined the fundamental surface reactions between Pb- and Mn-containing solids, the nature of these interactions at conditions relevant to drinking water supply and their implications for tap water quality had not been sufficiently explored. Such interactions can be important in affecting lead concentrations in drinking water. Recently, Trueman et al.[40] reported that without free chlorine, Mn(II) increased Pb release mainly because of the oxidation of lead by oxygen on MnO_2 deposits or by Mn(IV) itself. However, this may not be the scenario when free chlorine is present in the system. The goal of this work was to identify the products and pathways of the reaction of dissolved Mn(II), Pb(II) carbonate and free chlorine. Specific attention was paid to the heterogeneous catalytic effect of Mn solids on hydrocerussite and cerussite oxidation by chlorine. The oxidation of Pb(II) is a necessary step to form Pb(IV) oxide. This process may take place during drinking water distribution at locations where lead-containing materials and dissolved or solid Mn coexist. In this study, we investigated the oxidation of Pb(II) from Pb(II) carbonate solids with and without the presence of Mn(II) at various pH values. We performed batch experiments to probe the products and dynamics of the reactions, and these were supplemented by kinetic models based on mass balances and the stoichiometry of the reactions. Flow-through experiments provided additional information on reaction rates with a lower but sustained supply of free chlorine that is more directly relevant to the actual conditions in LSLs.

Materials and Methods

Materials

Hydrocerussite and cerussite were purchased from Sigma-Aldrich. A free chlorine stock solution was prepared using NaOCl (Fisher Chemical, 4-6% w/w) and ultrapure water. Plattnerite (β-PbO_2) was purchased from Acros Organics. Scrutinyite (α-PbO_2) was synthesized in a 500 mL polypropylene batch reactor with hydrocerussite as a precursor with the pH maintained at 10. The synthesis was conducted at carbonate-free conditions by sparging the solution with air that had been scrubbed of CO_2 using a 1 M NaOH solution. During the scrutinyite synthesis, the free chlorine concentration was maintained at 50 mg/L (0.70 mM) as Cl_2. The XRD pattern (Figure S1) confirmed the high purity of synthesized scrutinyite. Synthetic δ-MnO_2 (Figure S2) was prepared by reacting $KMnO_4$ with $MnCl_2$ at basic pH following a published method.[41,42] The identities of the solids synthesized were confirmed by X-ray diffraction (XRD). Reagent grade $NaHCO_3$, $NaNO_3$, NaOH, $MnCl_2$ and concentrated HNO_3 were purchased from Fisher Scientific. All solutions were prepared using ultrapure water (resistivity >18.2 MΩ-cm, Milli-Q, Millipore Corp., Milford, MA).

Experimental design

Three sets of batch experiments were conducted. To study cerussite or hydrocerussite oxidation in isolation, the first set of experiments were conducted with 200 mL of 2 mM cerussite or hydrocerussite suspensions with a DIC concentration of 0.2 mM (2.4 mg/L as C), 0.28 ± 0.03 mM free chlorine (20 ± 2 mg/L as Cl_2) and pH 6.5 to 8.5 ± 0.2 maintained by 0.1 M HNO_3 and 0.1 M NaOH. The high chlorine concentration was chosen to facilitate the development of a kinetic model for oxidation of Pb(II) in Pb(II) carbonate solids by free chlorine. A lower free chlorine concentration will yield a relatively short reaction time and we may not be able to capture some crucial features of the reactions in the batch experiment. To investigate the effect of an initial amount of scrutinyite and plattnerite on lead carbonate oxidation, the second set of experiments

had certain amounts of scrutinyite or plattnerite added to the suspensions of cerussite or hydrocerussite solutions with the same DIC, free chlorine, and pH as in the first set of experiments. In support of this second set of experiments, control experiments were conducted with just scrutinyite or plattnerite and free chlorine and no Pb(II) carbonate solids. In the third set of experiments, the effect of Mn(II) was studied by adding 0.1 or 1 mL of 0.25 M $MnCl_2$ solution to the cerussite or hydrocerussite suspensions to reach 0.1 mM or 1 M initial Mn(II) concentrations. All batch experiments were performed in 250 mL glass bottles with their contents stirred with polypropylene-coated stir bars at a speed of 500 rpm on a multi-position stirrer (VARIOMAG, Thermo, U.S.A) at room temperature (21 ± 1 °C).

For all batch experiments, 5 mL samples of suspension were collected at selected times. Reactions between solutes and the surfaces of solids were quenched by immediately filtering suspensions through 0.05 μm pore diameter polyethersulfone (PES) membranes (Tisch Scientific, U.S.A) with a collection of 2 mL of filtrate. Samples after this additional filtration step were acidified to 2% HNO_3 and preserved for dissolved lead analysis by ICP-MS. Samples of the suspension that included solids were collected at the beginning of the experiment and after 5 and 24 h of reaction. The suspensions were centrifuged and freeze-dried to yield solids for further analysis.

Flow-through experiments with suspensions of lead carbonate reacting with free chlorine were conducted in continuously stirred tank reactors (CSTRs). In contrast to the batch reactors in which free chlorine was added at a relatively high initial concentration, the flow-through reactors could provide a steady supply of free chlorine at a lower concentration that is more directly relevant to the drinking water supply. The reactions were examined both in the absence and presence of 0.1 mM δ-MnO_2 at the ambient room temperature (21 ± 1 °C). The δ-MnO_2 solid was employed

instead of Mn(II) solution in the flow-through experiments because any Mn(II) in the solution that was not oxidized by the initial influx of free chlorine would have been flushed out of the reactors (Figure S3). The volume of each reactor was 40 mL and lead carbonate suspensions were loaded to a concentration of 1 mM as Pb. Specific amounts of δ-MnO_2 that provided the same Pb:Mn ratio as a set of the batch experiments were added to CSTRs. Mixing was achieved by continuous stirring with a polypropylene-coated magnetic stir bar at 250 rpm. A 0.22 μm mixed cellulose filter membrane at the reactor outlet prevented the loss of solids from the reactor. Influent was pumped into the reactor at 2 mL/min using a peristaltic pump (Cole-Parmer), so the reactor hydraulic residence time (τ) was 20 min. The pH and free chlorine concentrations of the effluents were monitored, and aqueous samples were periodically collected for dissolved Pb(II) concentration analysis. The influents were prepared in 4-L polypropylene bottles covered with aluminum foil to minimize CO_2 exchange with the atmosphere and prevent photodegradation of free chlorine. Addition of an aliquot of 1 M $NaHCO_3$ solution to the bottles provided the DIC concentration of 0.02 mM (2.4 mg/L) as C. An aliquot of a NaOCl stock solution was added to reach a concentration of 0.034 mM (2.4 mg/L) as Cl_2. The pH was adjusted to the target values by addition of concentrated HNO_3 or freshly prepared 0.5 M NaOH solutions to reach pH 7.5 ± 0.2. The flow through experiments were conducted for 2000 min (i.e. 100 residence times).

Analytical methods

The residual free chlorine concentration was measured with the standard DPD method.[43] Dissolved lead was analyzed by inductively coupled plasma-mass spectrometry (ICP-MS) (PerkinElmer ELAN DRC II). Solution pH was measured with a glass pH electrode and pH meter (Accumet). XRD patterns were collected using Cu Kα radiation (Bruker d8 Advance X-ray diffractometer). Scanning Electron Microscopes (SEM) examination was performed with FEI Nova NanoSEM 230.

156 The specific surface areas of dry solids were determined by the Brunauer–Emmett–Teller-N_2
157 (BET- N_2) adsorption (Quantachrome Instruments) method.

158 **Model development:**

159 All the models were developed using constraints of mass balances and the stoichiometry of the
160 oxidation-reduction reactions. The specific rate equations used are presented in the Results and
161 Discussion section, and a brief overview of the modeling approach is provided here. The
162 conceptual model of the processes occurring is presented in Figure 2. The formation of PbO_2
163 included noncatalytic oxidation of Pb(II), autocatalytic oxidation of Pb(II) with PbO_2 formed *in*
164 *situ*, and catalytic oxidation of Pb(II) and Mn oxides. The consumption of free chlorine included
165 noncatalytic oxidation of Pb(II), autocatalytic oxidation of Pb(II) with PbO_2 formed *in situ*,
166 oxidation of Mn(II) to δ-MnO_2, and catalytic oxidation of Pb(II) with δ-MnO_2 formed *in situ*. In
167 this study, *in situ* means in the reactor. For cerussite and hydrocerussite oxidation, the consumption
168 of free chlorine was assumed to equal the formation of PbO_2 in molar concentration (reactions 1
169 and 2). For cerussite and hydrocerussite reaction with free chlorine in the presence of Mn, the
170 consumption of free chlorine included oxidation of Pb(II) as well as oxidation of Mn(II) (reaction
171 3). Mole balance equations were developed for free chlorine and PbO_2 that included terms for the
172 rates of oxidation of Pb(II) carbonate directly, catalyzed by PbO_2, and catalyzed by MnO_2. The pH
173 dependence was not accounted in model development since the data examined in comparison with
174 the model were all collected at pH 7.5 ± 0.2. For the flow-through experiment, the free chlorine in
175 the influent and δ-MnO_2 concentrations were treated as constants since it was continuously
176 supplied from a well mixed 4 L reservoir. Although catalytic reactions were surface-related
177 reactions, the surface area was incorporated into reaction rate constants in our model development.
178 Differential equations obtained from the mass balance equations were solved by MATLAB

R2018a. Optimization of the fit of data to model by adjusting multiple parameters at the same time to obtain the minimum coefficient of determination (R^2).

$$PbCO_3 + HOCl_{diss} + H_2O \leftrightarrow PbO_2 + HCO_{3\,diss}^- + Cl_{diss}^- + 2H^+ \quad (1)$$

$$Pb_3(CO_3)_2(OH)_2 + 3HOCl_{diss} + H_2O \leftrightarrow 3PbO_2 + 2HCO_{3\,diss}^- + 3Cl_{diss}^- + 5H^+ \quad (2)$$

$$Mn_{diss}^{2+} + HOCl_{diss} + H_2O \leftrightarrow \delta - MnO_2 + Cl_{diss}^- + 3H^+ \quad (3)$$

Results and Discussion

The catalytic effect of PbO_2 on lead carbonate oxidation

The trends in the consumption of free chlorine for oxidation of cerussite provided insights into an autocatalytic reaction in which the production of an initial amount of PbO_2 accelerated the rate of further PbO_2 formation (Figure 3). We observed the oxidation occurring with a lag stage followed by a rapid stage for both cerussite and hydrocerussite. These two stages of oxidation for lead carbonate were also observed by other researchers.[16] The addition of PbO_2 (either plattnerite or scrutinyite) accelerated cerussite oxidation by free chlorine and dramatically shortened the lag stage of the reaction (Figure 3). With the increasing amount of PbO_2 (from 0.5 to 1 g/L), the free chlorine consumption speed increased, indicating the increasing rate of cerussite oxidation. A shortened lag stage was still observed with high PbO_2 concentration (1 g/L). Control experiments determined that plattnerite and scrutinyite by themselves did not accelerate chlorine degradation (Figure S4). While the data presented in Figure 3 are for cerussite, similar trends were observed for hydrocerussite and are shown in the supporting information (Figure S6).

When comparing the rate of chlorine consumption associated with oxidation of cerussite and hydrocerussite, the rate was faster with hydrocerussite (Figure S6), which was consistent with

200 previous findings.[16,44] The lower oxidation speed of cerussite by free chlorine may due to
201 cerussite's lower specific surface area (3.28 m^2/g versus 10.70 m^2/g for hydrocerussite) that may
202 be related to lower concentration of active surface sites for oxidation or to a slower release of
203 dissolved Pb(II) from the Pb(II) carbonate solid.

204 Kinetic models were developed to interpret the rates of cerussite and hydrocerussite oxidation
205 under the experimental conditions. For cerussite and hydrocerussite oxidation with or without
206 initial PbO_2 (scrutinyite or plattnerite), the consumption of free chlorine included noncatalytic
207 oxidation of Pb(II) and autocatalytic oxidation of Pb(II) with PbO_2 added or formed *in situ*
208 (equation 1). The moles of PbO_2 formed were the same as the moles of free chlorine consumed
209 (equation 2). For Pb(II) carbonate oxidation without any added PbO_2, the consumption of free
210 chlorine and the formation of PbO_2 were described as simplified forms of equations 1 and 2 with
211 a value of zero for $[Pb(IV)_{added}]$ which eliminated particular terms in the equations. The term
212 [HOCl] indicates all free chlorine (both HOCl and OCl^-). Good fits of the model to the data
213 required different rate constants for Pb(II) oxidation catalyzed by PbO_2 formed *in situ* versus PbO_2
214 added as pre-synthesized solids. An initial modeling effort attempted to interpret the data using a
215 single rate constant for PbO_2, but this provided much poorer fits (equations S1-S4 and Figure S5).
216 The kinetic constants k_1^* and k_2^* correspond to the noncatalytic and autocatalytic reaction proposed
217 in other studies.[8,16,45] The catalytic reaction rate constants (k_2^*, k_3^*, and k_4^*) were the value of
218 apparent rate constants k_2, k_3, and k_4 multiplied by the amount of PbO_2 in the system (equations 3
219 and 4). The added scrutinyite and plattnerite were assumed to have different catalytic reaction rate
220 constants (k_3^* and k_4^*, respectively). Equations 1-5 were employed for kinetic model development
221 with scrutinyite and equations S5-S9 were used with plattnerite. The four unknown constants were
222 estimated by finding the values that provided the optimal fit of five sets of experimentally

measured chlorine consumption data (Figure 3 and Figure S6). The definition and unit of each constant are listed in Table 1. These constants in Table 1 are apparent rate constants for oxidation reactions. The dissolution of lead carbonate solids and adsorption of Pb(II) onto PbO_2 or δ-MnO_2 were not considered in the model development because they are much faster compared with the oxidation reactions so they can be ignored.

$$-\frac{d[HOCl]}{dt} = k_1^* * [Pb(II)_{lead\ carbonate}] * [HOCl] + k_2^* * [Pb(II)_{lead\ carbonate}] * [HOCl] + k_3^* * [Pb(II)_{lead\ carbonate}] * [HOCl] \quad (1)$$

$$\frac{d[Pb(IV)]}{dt} = k_1^* * [Pb(II)_{lead\ carbonate}] * [HOCl] + k_2^* * [Pb(II)_{lead\ carbonate}] * [HOCl] + k_3^* * [Pb(II)_{lead\ carbonate}] * [HOCl] \quad (2)$$

$$k_2^* = k_2 * [Pb(IV)] \quad (3)$$

$$k_3^* = k_3 * [Pb(IV)_{added}] \quad (4)$$

$$[Pb(II)_{lead\ carbonate}] = [Pb(II)_0] - [Pb(IV)] \quad (5)$$

The constants that provided the best fit of the model output to the experimental results are compiled in Table 2. The simulated free chlorine concentration trends based on these reactions and apparent constants are shown together with the experimental data in Figure 3 (cerussite) and Figure S6 (hydrocerussite). The apparent constant for cerussite oxidation on PbO_2 formed *in situ* ($k_2 = 5.5\times10^5$ $M^{-2}\cdot h^{-1}$) was two orders of magnitude higher than the constants for Pb(II) oxidation on the added PbO_2 ($k_3 = 6\times10^3$ $M^{-2}\cdot h^{-1}$ and $k_4 = 6\times10^3$ $M^{-2}\cdot h^{-1}$). The apparent constants for hydrocerussite followed the same trend. The oxidation rate constants k_2^* - k_4^* were calculated by multiplying k_2 - k_4 by the concentration of PbO_2 present (equations 3, 4, and S8). The rate constants used here are related to the moles of PbO_2 present, but for surface-based reactions, the

244 controlling factor is probably the surface area of PbO_2 present. The higher specific surface area of
245 PbO_2 formed *in situ* may be one reason for its more robust catalytic effect on Pb(II) carbonate
246 oxidation than that of pre-synthesized PbO_2. Unfortunately, we did not have a means of measuring
247 the surface area of PbO_2 formed *in situ*. Comparing hydrocerussite and cerussite, hydrocerussite
248 exhibited a higher autocatalytic oxidation speed than cerussite and k_1* and k_2 of hydrocerussite
249 were both greater than these of cerussite. The reaction rate constants k_1^* and apparent rate constants
250 k_3 and k_4 in Table 2 were almost 10 times higher than in the study by Liu et al.[16] because the
251 surface areas of cerussite and hydrocerussite (3.38 and 10.70 m^2/g) employed in this study were
252 almost 10 times higher than Liu et al.[16] (0.42 and 0.81 m^2/g).

253 The effect of pH on cerussite oxidation was examined (Figure 4). The duration of the lag
254 stage was not affected by increasing pH for cerussite. Free chlorine consumption speeds were
255 almost the same at pH 6.5, 7.5, and 8.5 for cerussite. For hydrocerussite oxidation, the free chlorine
256 consumption speed decreased with increasing pH (Figure S7). Similar results were observed by
257 Zhang and Lin.[42] The influence of pH on Pb(II) carbonate oxidation by free chlorine could be
258 related to two phenomena. First, the pH determines the ratio of $HOCl/OCl^-$, and for many species,
259 oxidation rates are faster with HOCl than with OCl^-.[46] Second, the pH determines the species of
260 dissolved Pb(II), which also affects the oxidation rates according to Figure 3. Prior research
261 demonstrated that high DIC concentration could inhibit Pb(II) carbonate oxidation by free chlorine
262 via formation of dissolved Pb(II) carbonate complexes, which are much less reactive compared
263 with lead hydroxo complexes.[8,16,44]

264 *The catalytic effect of Mn oxide on lead carbonate oxidation*

The addition of Mn(II) significantly enhanced the rate of cerussite oxidation (Figure 5). With free chlorine Mn(II), oxidation was much faster than Pb(II) oxidation and it produced δ-MnO_2 (Figure S2). The free chlorine concentration was in excess of the amount required to oxidize 0.1 mM Mn(II), so after Mn(II) was completely oxidized, there was still sufficient free chlorine to oxidize Pb(II) carbonate. The rate of Pb(II) carbonate oxidation was accelerated as the rate of free chlorine consumption was much higher than with the lead carbonate oxidation in the absence of Mn(II). Hydrocerussite oxidation with the presence of Mn(II) showed the same trends as cerussite (Figure S9).

A kinetic model for free chlorine concentration during Pb(II) oxidation in systems to which Mn(II) had been added was developed (equations 6 and 7). Because the rate of Mn(II) oxidation was at least 3 orders of magnitude higher than the rates of other reactions used in the model, we assumed that all of the Mn(II) was instantaneously oxidized to δ-MnO_2; efforts to account for the kinetics of Mn(II) oxidation made the model more complicated but did not improve the ability to simulate Pb(II) oxidation. This assumption was confirmed by the similar catalytic effects on Pb(II) carbonate oxidation of δ-MnO_2 solids formed *in situ* and added (Figure 5, S8, and S9). In developing the model of Pb(II) oxidation in the presence of Mn oxide, the constants for non-catalytic Pb(II) oxidation and for oxidation catalyzed by PbO_2 were set at the values determined from the previously discussed experiments in which no Mn had been added. k_5 value was determined by fitting the model output to experimental data of chlorine consumption in the presence of 0.1 mM Mn(II). The value obtained then can be successfully applied to the system with 1mM Mn(II) (Figure 5). The definition and units of each constant are listed in Table 1. The actual second order oxidation rate constants were determined using apparent constants as noted in equation 7.

$$\frac{d[Pb(IV)]}{dt} = k_1^* * [Pb(II)_{lead\ carbonate}] * [HOCl] + k_2^* * [Pb(IV)] * [Pb(II)_{lead\ carbonate}] * [HOCl] + k_5^* * [Pb(II)_{lead\ carbonate}] * [HOCl] \quad (6)$$

$$k_5^* = k_5 * [\delta - MnO_2] \quad (7)$$

Based on our modeling results (Table 2), the apparent constants for Pb(II) oxidation with δ-MnO_2 were one order of magnitude higher than these of PbO_2 formed *in situ*. Considering the amount of δ-MnO_2 in the system, the actual catalytic rate constant with δ-MnO_2 could be at least 3 orders of magnitude higher than that of PbO_2 formed *in situ* and PbO_2 added. Apart from the catalytic effect of Mn(II) on Pb(II) carbonate oxidation, we also observed faster chlorine consumption rates for Mn(II) when Pb(II) carbonate was present than when Mn(II) was present on its own, which may indicate that the surface of Pb(II) carbonate helped catalyze the oxidation of Mn(II) by chlorine.

Products of Pb(II) carbonate oxidation

The reaction of cerussite and hydrocerussite with free chlorine produced PbO_2. Scrutinyite was formed from lead carbonate oxidation as determined by XRD (Figure 6). The effect of Mn(II) on lead carbonate oxidation by free chlorine was further confirmed by XRD patterns. The structural changes of Pb(II) carbonate solids and the formation of PbO_2 were also observed by SEM results (Figure S10). With 1 mM Mn(II), there was no change in the cerussite XRD pattern because all the free chlorine was consumed by Mn(II) oxidation. For cerussite oxidation by free chlorine, the XRD patterns for 5 h samples were almost the same as those of the initial cerussite, which was consistent with batch experiment results that the reactions were in a lag stage for the first 5 h. After 24 h reaction with free chlorine, peaks for scrutinyite at 2θ of 23° and 28° were observed for the reacted cerussite. Liu et al.[16] examined cerussite and hydrocerussite oxidation by

310 50 mg/L free chlorine and observed the signature peaks for scrutinyite at a longer oxidation time,
311 which was probably because of the higher DIC concentration (0.001 M) used in their experiments.

312 With the presence of Mn(II), the same peaks for scrutinyite were observed after cerussite
313 reaction with free chlorine for both 5 h and 24 h. These XRD results were consistent with the
314 observed free chlorine consumption profiles from batch experiments. As shown in Figure 6,
315 scrutinyite was the only product of cerussite oxidation by free chlorine. The same overall trend
316 was observed for hydrocerussite oxidation (Figure S11); with the addition of 0.1 mM Mn(II),
317 scrutinyite was observed in the solid sample for 5 h and 24 h reaction with free chlorine. The
318 formation of pure scrutinyite from hydrocerussite oxidation was also observed in the studies by
319 Wang et al.[8] and Liu et al.[16] When starting with cerussite and no DIC, Wang et al.[8] observed
320 cerussite transformed to hydrocerussite after one day and a mixture of scrutinyite and plattnerite
321 formed after 28 days. Nevertheless, in both the work of Liu et al.[16] and our research, plattnerite
322 was not observed after cerussite oxidation. The difference in these studies may be due to difference
323 in experimental pH and carbonate concentration. Higher pH and higher carbonate concentration
324 can lead to higher generation of scrutinyite over plattnerite in PbO_2 formation. We also note that
325 there are two possible processes for the oxidation of lead carbonate solids to PbO_2, dissolution–
326 oxidation-reprecipitation (DOR) and direct solid-state oxidation.[8,16,47] In this study, DOR is
327 considered to be the main PbO_2 formation pathways. Although there might be direct solid-state
328 oxidation of a Pb(II) layer at the surface of lead carbonate solids, this process will yield a protective
329 layer of PbO_2 on lead carbonate solid surface and inhibit further oxidation. Nevertheless, thorough
330 oxidation of Pb(II) carbonate solids to PbO_2 was observed by previous studies[8,48], which indicates
331 that DOR is more significant.

Flow-through experiment

In the batch experiments, a high free chlorine concentration (0.28 ± 0.03 mM as Cl_2) was applied initially and then depleted as it oxidized Pb(II) and Mn(II) species. In contrast to the batch experiments, flow-through experiments were conducted with a more realistic free chlorine concentration (0.034 mM or 2.4 mg/L as Cl_2) that was continuously supplied. The oxidation of cerussite was enhanced with δ-MnO_2 in the flow-through experiment (Figure 7). After a period of relatively high effluent concentrations (~1.5 μM) of Pb(II) as the CSTRs started up, the concentrations of Pb(II) dropped to much lower values (0.05-0.32 μM). The effluent concentrations of Pb(II) were lower with δ-MnO_2 (0.05 μM) than without (0.32 μM). For the system without δ-MnO_2, the concentrations of Pb(II) stabilized at a steady-state concentration. A steady-state was not necessarily expected since the rate of Pb(II) consumption would be expected to increase as more PbO_2 accumulated in the reactor; however, the rate of PbO_2 accumulation may have been slow enough for the system to be at steady-state. For the system with δ-MnO_2, a steady state was not reached and Pb(II) concentrations decreased over the duration of the experiment, which indicates that the amount of PbO_2 in the system was probably increasing with time. The faster oxidation of cerussite with δ-MnO_2 was also confirmed by higher chlorine consumption in the effluent. When similar experiments were conducted with hydrocerussite (Figure S12), we observed the similar trend that δ-MnO_2 accelerates hydrocerussite oxidation.

For model development, we considered the conditions with and without δ-MnO_2 (equations 8 and 9). Q and V are the flow rate and volume, respectively. The amount of Pb(II) (≤ 1.2 μmol) in the total outlet was neglected in the model development because it was negligible when compared with the amount of Pb(II) and Pb(IV) solids (≥ 38.8 μmol) left in the CSTRs after the experiment. For cerussite oxidation without δ-MnO_2, the δ-MnO_2 concentration was set to zero in

equations 8 and 9 which eliminated particular terms in the equations. The constants were defined in Table 1, and rate constants (k_1^*, k_2^*, and k_5^*) were obtained by using the same rate constants obtained from batch experiments (Table 2). The application of parameters from batch experiments to flow-through experiment was based on the hypothesis that the behavior of solids in batch experiment was consistent with the behavior of solids in the flow-through experiments, which was confirmed by the overall agreement between experimental and modeled chlorine concentrations in the effluent. Chlorine concentration profiles in the effluent derived from modeling work ae shown in Figure 7 and Figure S11 as dashed lines. The simulations provided general agreement with the flow-through experimental data that the presence of δ-MnO_2 accelerates chlorine consumption, which indicates a higher rate of Pb(II) oxidation.

$$\frac{d[HOCl]}{dt} * V = [HOCl_{inlet}] * Q - \{k_1^* * [Pb(II)_{lead\ carbonate}] * [HOCl] - k_2^* * [Pb(II)_{lead\ carbonate}] * [HOCl] - k_5^* * [Pb(II)_{lead\ carbonate}] * [HOCl]\} * V - [HOCl] * Q \quad (8)$$

$$\frac{d[Pb(IV)]}{dt} = k_1^* * [Pb(II)_{lead\ carbonate}] * [HOCl] + k_2^* * [Pb(II)_{lead\ carbonate}] * [HOCl] + k_5^* * [Pb(II)_{lead\ carbonate}] * [HOCl] \quad (9)$$

Environmental Implications

PbO_2 solids can maintain low dissolved Pb(II) concentrations, but they are not always observed on LSLs that deliver drinking water with free chlorine as the disinfectant. Water chemistry can strongly influence the oxidation of Pb(II) carbonate in the actual distribution system. Under a more realistic and continuously supplied free chlorine concentration (0.034 mM or 2.4 mg/L as Cl_2), δ-MnO_2 also enhanced Pb(II) carbonate oxidation.

The effect of Mn on Pb(II) carbonate oxidation can be successfully explained by the δ-MnO_2 that formed *in situ* acting as a heterogeneous catalyst for Pb(II) oxidation. Modeling work showed

that the catalytic effect of δ-MnO_2 formed *in situ* is almost three orders of magnitude faster than that of an equal amount of PbO_2 formed *in situ*. Although results in this study were obtained from batch and flow-through experiments, it can be extrapolated to LSLs. In a pipe reactor study by Bae et al.,[49] an accidental dosage of Mn(II) was found to skyrocket the free chlorine consumption speed and decrease the Pb(II) concentration from ~50 μg/L to less than 10 μg/L in the effluent of lead pipes. Our experimental and modeling results can help explain the phenomenon of Pb(II) decreasing in the effluent of lead pipes by PbO_2 formation catalyzed by in situ formation of MnO_2. We anticipate that the study of water chemistry in bench-scale experiments can be employed to study the Pb corrosion in drinking water distribution systems with different levels of Mn in the water. The same findings may potentially be extended to other metal oxide deposits on the inner surface of LSLs, such as those of iron and copper. Nevertheless, the catalytic effect of these metal oxide may not as robust as δ-MnO_2, which has a relative high surface area, fast Pb(II) adsorption kinetics, and high Pb(II) adsorption capacity.[50] Furthermore, our findings likely have broader implications for the role of deposits (such as Mn, Fe, and Cu oxide) in drinking water distribution systems. Previous studies have explored the role of these deposits as sinks for trace inorganic contaminants (arsenic, selenium, vanadium, etc.) via sorption process.[11,14,51,52] Here, our findings reveal another possible role of these deposits in mediating redox transformations of trace inorganic contaminants such as Pb(II).

Supporting Information

One table and twelve figures show the initial model development for Pb(II) carbonate oxidation with added PbO_2, standard reduction potentials of chemicals in the experiment, XRD patterns for synthesized scrutinyite and solids obtained from Mn(II) oxidation, flow-through experiment set-up, chlorine concentration with PbO_2, free chlorine concentration profiles for hydrocerussite

oxidation with and without PbO_2, the effect of pH on hydrocerussite oxidation by chlorine, oxidation of Pb(II) carbonate by chlorine with and without 0.1 mM δ-MnO_2 solids, oxidation of hydrocerussite by chlorine with different Mn(II) concentrations, SEM images of Pb(II) carbonate before and after reactions, XRD patterns for of solids from hydrocerussite oxidation experiments, and results of flow-through experiments with hydrocerussite.

Author information

Corresponding Author

*pan10@llnl.gov. Phone: (314) 608-8987; 7000 East Avenue, Livermore, CA 94550. (C.P.)

Acknowledgments

This research was supported by the U.S. National Science Foundation (CBET 1603717, CHE 1709484). W.P. acknowledges the fellowship support through the McDonnell International Scholars Academy. This work was performed in part using the Nanoscale Research Facility at Washington University in St. Louis. Work at LLNL was conducted under the auspices of the US Department of Energy at LLNL under Contract DE-AC52-07NA27344. We thank Anushka Mishrra, Anshuman Satpathy, and Neha Sharma for assistance with experimental activities.

415 **Reference**

416 (1) Edwards, M.; Triantafyllidou, S.; Best, D. Elevated Blood Lead in Young Children Due
417 to Lead-Contaminated Drinking Water: Washington, DC, 2001−2004. *Environ. Sci. Technol.*
418 **2009**, *43* (5), 1618–1623.

419 (2) Edwards, M. Fetal Death and Reduced Birth Rates Associated with Exposure to Lead-
420 Contaminated Drinking Water. *Environ. Sci. Technol.* **2013**, *48* (1), 739–746.

421 (3) Triantafyllidou, S.; Edwards, M. Lead (Pb) in Tap Water and in Blood: Implications for
422 Lead Exposure in the United States. *Crit. Rev. Environ. Sci. Technol.* **2012**, *42* (13), 1297–1352.

423 (4) U.S. EPA, Maximum Contaminant Level Goals and National Primary Drinking Water
424 Regulations for Lead and Copper. Final Rule. Fed. Regist. 1991, *56*, 26460

425 (5) Rosario-Ortiz, F.; Rose, J.; Speight, V.; Von Gunten, U.; Schnoor, J. How Do You like
426 Your Tap Water? *Science.* **2016**, *351* (6276), 912–914.

427 (6) Cornwell, D. A.; Brown, R. A.; Via, S. H. National Survey of Lead Service Line
428 Occurrence. *J. Am. Water Works Assoc.* **2016**, *108* (4), E182–E191.
429 https://doi.org/10.5942/jawwa.2016.108.0086.

430 (7) Schock, M. R. Understanding Corrosion Control Strategies for Lead. *J. Am. Water Works*
431 *Assoc.* **1989**, *81* (7), 88–100.

432 (8) Wang, Y.; Xie, Y.; Li, W.; Wang, Z.; Giammar, D. E. Formation of Lead(IV) Oxides
433 from Lead(II) Compounds. *Environ. Sci. Technol.* **2010**, *44* (23), 8950–8956.

434 (9) Del Toral, M. A.; Porter, A.; Schock, M. R. Detection and Evaluation of Elevated Lead

435 Release from Service Lines: A Field Study. *Environ. Sci. Technol.* **2013**, *47* (16), 9300–9307.
436 https://doi.org/10.1021/es4003636.

437 (10) DeSantis, M. K.; Triantafyllidou, S.; Schock, M. R.; Lytle, D. A. Mineralogical Evidence
438 of Galvanic Corrosion in Drinking Water Lead Pipe Joints. *Environ. Sci. Technol.* **2018**, *52* (6),
439 3365–3374. https://doi.org/10.1021/acs.est.7b06010.

440 (11) Peng, C. Y.; Korshin, G. V; Valentine, R. L.; Hill, A. S.; Friedman, M. J.; Reiber, S. H.
441 Characterization of Elemental and Structural Composition of Corrosion Scales and Deposits
442 Formed in Drinking Water Distribution Systems. *Water Res.* **2010**, *44* (15), 4570–4580.

443 (12) Kim, E. J.; Herrera, J. E. Characteristics of Lead Corrosion Scales Formed during
444 Drinking Water Distribution and Their Potential Influence on the Release of Lead and Other
445 Contaminants. *Environ. Sci. Technol.* **2010**, *44* (16), 6054–6061.
446 https://doi.org/10.1021/es101328u.

447 (13) Frenkel, A. I.; Korshin, G. V. EXAFS Studies of the Chemical State of Lead and Copper
448 in Corrosion Products Formed on the Brass Surface in Potable Water. *J. Synchrotron Radiat.*
449 **1999**, *6* (3), 653–655.

450 (14) Schock, M. R.; Hyland, R. N.; Welch, M. M. Occurrence of Contaminant Accumulation
451 in Lead Pipe Scales from Domestic Drinking-Water Distribution Systems. *Environ. Sci. Technol.*
452 **2008**, *42* (12), 4285–4291. https://doi.org/10.1021/es702488v.

453 (15) Vasquez, F. A.; Heaviside, R.; Tang, Z.; Taylor, J. S. Effect of Free Chlorine and
454 Chloramines on Lead Release in a Distribution System. *J. Am. Water Works Assoc.* **2006**, *98* (2),
455 144–154.

(16) Liu, H.; Korshin, G. V; Ferguson, J. F. Investigation of the Kinetics and Mechanisms of the Oxidation of Cerussite and Hydrocerussite by Chlorine. *Environ. Sci. Technol.* **2008**, *42* (9), 3241–3247.

(17) Noel, J. D.; Wang, Y.; Giammar, D. E. Effect of Water Chemistry on the Dissolution Rate Ofthe Lead Corrosion Product Hydrocerussite. *Water Res.* **2014**, *54*, 237–246. https://doi.org/10.1016/j.watres.2014.02.004.

(18) Triantafyllidou, S.; Schock, M. R.; DeSantis, M. K.; White, C. Low Contribution of PbO_2 -Coated Lead Service Lines to Water Lead Contamination at the Tap. *Environ. Sci. Technol.* **2015**, *49* (6), 3746–3754. https://doi.org/10.1021/es505886h.

(19) Dryer, D. J.; Korshin, G. V. Investigation of the Reduction of Lead Dioxide by Natural Organic Matter. *Environ. Sci. Technol.* **2007**, *41* (15), 5510–5514. https://doi.org/10.1021/es070596r.

(20) Lin, Y.-P.; Valentine, R. L. Release of Pb(II) from Monochloramine-Mediated Reduction of Lead Oxide (PbO_2). *Environ. Sci. Technol.* **2008**, *42* (24), 9137–9143. https://doi.org/10.1021/es801037n.

(21) Lin, Y.-P.; Valentine, R. L. Reductive Dissolution of Lead Dioxide (PbO_2) in Acidic Bromide Solution. *Environ. Sci. Technol.* **2010**, *44* (10), 3895–3900. https://doi.org/10.1021/es100133n.

(22) Wang, Y.; Wu, J.; Giammar, D. E. Kinetics of the Reductive Dissolution of Lead(IV) Oxide by Iodide. *Environ. Sci. Technol.* **2012**, *46* (11), 5859–5866. https://doi.org/10.1021/es2038905.

(23) Lin, Y.-P.; Washburn, M. P.; Valentine, R. L. Reduction of Lead Oxide (PbO_2) by Iodide and Formation of Iodoform in the PbO_2/I^-/NOM System. *Environ. Sci. Technol.* **2008**, *42* (8), 2919–2924. https://doi.org/10.1021/es702797b.

(24) Shi, Z.; Stone, A. T. PbO_2(s, Plattnerite) Reductive Dissolution by Natural Organic Matter: Reductant and Inhibitory Subfractions. *Environ. Sci. Technol.* **2009**, *43* (10), 3604–3611.

(25) Shi, Z.; Stone, A. T. PbO_2 (s, Plattnerite) Reductive Dissolution by Aqueous Manganous and Ferrous Ions. *Environ. Sci. Technol.* **2009**, *43* (10), 3596–3603.

(26) Edwards, M.; Dudi, A. Role of Chlorine and Chloramine in Corrosion of Lead-Bearing Plumbing Materials. *J. Am. Water Works Assoc.* **2004**, 96(10), 69–81. https://doi.org/10.2307/41311235.

(27) Sly, L. I.; Hodgkinson, M. C.; Arunpairojana, V. Deposition of Manganese in a Drinking Water Distribution System. *Appl. Environ. Microbiol.* **1990**, *56* (3), 628–639.

(28) Kohl, P. M.; Medlar, S. J. *Occurrence of Manganese in Drinking Water and Manganese Control*; American Water Works Association, 2006.

(29) Gerke, T. L.; Little, B. J.; Maynard, J. B. Manganese Deposition in Drinking Water Distribution Systems. *Sci. Total Environ.* **2016**, *541*, 184–193.

(30) Gallard, H.; Allard, S.; Nicolau, R.; Von Gunten, U.; Croué, J. P. Formation of Iodinated Organic Compounds by Oxidation of Iodide-Containing Waters with Manganese Dioxide. *Environ. Sci. Technol.* **2009**, *43* (18), 7003–7009.

(31) Tebo, B. M.; Bargar, J. R.; Clement, B. G.; Dick, G. J.; Murray, K. J.; Parker, D.; Verity, R.; Webb, S. M. Biogenic Manganese Oxides: Properties and Mechanisms of Formation. *Annu.*

498 *Rev. Earth Planet. Sci.* **2004**, *32* (1), 287–328.
499 https://doi.org/10.1146/annurev.earth.32.101802.120213.

500 (32) Zacheus, O. M.; Lehtola, M. J.; Korhonen, L. K.; Martikainen, P. J. Soft Deposits, the
501 Key Site for Microbial Growth in Drinking Water Distribution Networks. *Water Res.* **2001**, *35*
502 (7), 1757–1765. https://doi.org/10.1016/S0043-1354(00)00431-0.

503 (33) Szewzyk, U.; Szewzyk, R.; Manz, W.; Schleifer, K.-H. Microbiological Safety of
504 Drinking Water. *Annu. Rev. Microbiol.* **2000**, *54* (1), 81–127.
505 https://doi.org/10.1146/annurev.micro.54.1.81.

506 (34) Cerrato, J. M.; Falkinham, J. O.; Dietrich, A. M.; Knocke, W. R.; McKinney, C. W.;
507 Pruden, A. Manganese-Oxidizing and -Reducing Microorganisms Isolated from Biofilms in
508 Chlorinated Drinking Water Systems. *Water Res.* **2010**, *44* (13), 3935–3945.
509 https://doi.org/10.1016/J.WATRES.2010.04.037.

510 (35) Marcus, D. N.; Pinto, A.; Anantharaman, K.; Ruberg, S. A.; Kramer, E. L.; Raskin, L.;
511 Dick, G. J. Diverse Manganese(II)-Oxidizing Bacteria Are Prevalent in Drinking Water Systems.
512 *Environ. Microbiol. Rep.* **2017**, *9* (2), 120–128. https://doi.org/10.1111/1758-2229.12508.

513 (36) Zhao, D.; Yang, X.; Zhang, H.; Chen, C.; Wang, X. Effect of Environmental Conditions
514 on Pb (II) Adsorption on β-MnO_2. *Chem. Eng. J.* **2010**, *164* (1), 49–55.

515 (37) Xu, M.; Wang, H.; Lei, D.; Qu, D.; Zhai, Y.; Wang, Y. Removal of Pb(II) from Aqueous
516 Solution by Hydrous Manganese Dioxide: Adsorption Behavior and Mechanism. *J. Environ. Sci.*
517 **2013**, *25* (3), 479–486. https://doi.org/10.1016/S1001-0742(12)60100-4.

518 (38) Eren, E.; Gumus, H.; Sarihan, A. Synthesis, Structural Characterization and Pb(II)

519 Adsorption Behavior of K- and H-Birnessite Samples. *Desalination* **2011**, *279* (1–3), 75–85.
520 https://doi.org/10.1016/J.DESAL.2011.05.058.

521 (39) Matocha, C. J.; Elzinga, E. J.; Sparks, D. L. Reactivity of Pb(II) at the Mn(III,
522 IV)(Oxyhydr) Oxide−Water Interface. *Environ. Sci. Technol.* **2001**, *35* (14), 2967–2972.

523 (40) Trueman, B. F.; Gregory, B. S.; McCormick, N. E.; Gao, Y.; Gora, S.; Anaviapik-Soucie,
524 T.; L'Hérault, V.; Gagnon, G. A. Manganese Increases Lead Release to Drinking Water.
525 *Environ. Sci. Technol.* **2019**, *53* (9), 4803–4812. https://doi.org/10.1021/acs.est.9b00317.

526 (41) Villalobos, M.; Toner, B.; Bargar, J.; Sposito, G. Characterization of the Manganese
527 Oxide Produced by *Pseudomonas Putida* Strain MnB1. *Geochim. Cosmochim. Acta* **2003**, *67*
528 (14), 2649–2662.

529 (42) Pan, C.; Liu, H.; Catalano, J. G.; Qian, A.; Wang, Z.; Giammar, D. E. Rates of Cr(VI)
530 Generation from $Cr_xFe_{1-x}(OH)_3$ Solids upon Reaction with Manganese Oxide. *Environ. Sci.*
531 *Technol.* **2017**, *51* (21), 12416–12423.

532 (43) Clesceri, L. S.; Greenberg, A. E.; Eaton, A. D. *Standard Methods for the Examination of*
533 *Water and Wastewater*, 20th ed.;American Public Health Association, American Water Works
534 Association, Water Environment Federation: Washington, DC, 1999.

535 (44) Zhang, Y.; Lin, Y.-P. Determination of PbO_2 Formation Kinetics from the Chlorination
536 of Pb(II) Carbonate Solids via Direct PbO_2 Measurement. *Environ. Sci. Technol* **2011**, *45*, 30.
537 https://doi.org/10.1021/es1039826.

538 (45) Brezonik, P. *Chemical Kinetics and Process Dynamics in Aquatic Systems*; Routledge,
539 2018.

(46) Nadupalli, S.; Koorbanally, N.; Jonnalagadda, S. B. Kinetics and Mechanism of the Oxidation of Amaranth with Hypochlorite. *J. Phys. Chem. A* **2011**, *115* (27), 7948–7954. https://doi.org/10.1021/jp202812f.

(47) Liu, H.; Korshin, G. V.; Ferguson, J. F. Interactions of Pb(II)/Pb(IV) Solid Phases with Chlorine and Their Effects on Lead Release. *Environ. Sci. Technol.* **2009**, *43* (9), 3278–3284. https://doi.org/10.1021/es803179b.

(48) Lytle, D. A.; Schock, M. R. Formation of Pb(IV) Oxides in Chlorinated Water. *J. Am. Water Works Assoc.* **2005**, *97* (11), 102–114.

(49) Bae, Y.; Giammar, D.; Ivarson, A.; Mishrra, A.; Pasteris, J.; Schattner, L. The Ability of Orthophosphate to Limit Lead Release from Pipe Scales When Switching from Free Chlorine to Monochloramine. In *2018 Water Quality Technology Conference*; 2018.

(50) McKenzie, R. The Adsorption of Lead and Other Heavy Metals on Oxides of Manganese and Iron. *Aust. J. Soil Res.* **1980**, *18* (1), 61. https://doi.org/10.1071/SR9800061.

(51) Hill, A. S.; Friedman, M. J.; Reiber, S. H.; Korshin, G. V.; Valentine, R. L. Behavior of Trace Inorganic Contaminants in Drinking Water Distribution Systems. *J. Am. Water Works Assoc.* **2010**, *102* (7), 107–118. https://doi.org/10.1002/j.1551-8833.2010.tb10153.x.

(52) Gerke, T. L.; Scheckel, K. G.; Schock, M. R. Identification and Distribution of Vanadinite ($Pb_5(V^{5+}O_4)_3Cl$) in Lead Pipe Corrosion By-Products. *Environ. Sci. Technol.* **2009**, *43* (12), 4412–4418. https://doi.org/10.1021/es900501t.

560 **Table 1 Definitions and units for constants in kinetic model.**

Constants	Definitions	Units
*$[HOCl]_0$	Initial free chlorine concentration	mM
$Pb(II)_0$	Initial Pb(II) carbonate concentrations	mM
$Pb(IV)_{add}$	The concentration of Pb(IV) solids added	mM
δ-MnO_2	The concentration of Mn(IV) formed in the batch experiments	mM
k_1^*	Rate constant of homogeneous Pb(II) carbonate oxidation by chlorine	$M^{-1}\cdot h^{-1}$
k_2^*	Rate constant for heterogeneous Pb(II) carbonate oxidation by chlorine catalyzed by PbO_2 generated *in situ*	$M^{-1}\cdot h^{-1}$
k_3^*	Rate constant for heterogeneous Pb(II) carbonate oxidation by chlorine catalyzed by scrutinyite	$M^{-1}\cdot h^{-1}$
k_4^*	Rate constant for heterogeneous Pb(II) carbonate oxidation by chlorine catalyzed by plattnerite	$M^{-1}\cdot h^{-1}$
k_5^*	Rate constant for heterogeneous Pb(II) carbonate oxidation by chlorine catalyzed by manganese oxide	$M^{-1}\cdot h^{-1}$
k_2	Apparent constant for heterogeneous Pb(II) carbonate oxidation by chlorine catalyzed by PbO_2 generated *in situ*	$M^{-2}\cdot h^{-1}$
k_3	Apparent constant for heterogeneous Pb(II) carbonate oxidation by chlorine catalyzed by scrutinyite	$M^{-2}\cdot h^{-1}$
k_4	Apparent constant for heterogeneous Pb(II) carbonate oxidation by chlorine catalyzed by plattnerite	$M^{-2}\cdot h^{-1}$
k_5	Apparent constant for heterogeneous Pb(II) carbonate oxidation by chlorine catalyzed by manganese oxide	$M^{-2}\cdot h^{-1}$

561

562 **Table 2. Constants for modeling the dynamics of HClO during Pb(II) carbonate oxidation at**

563 **pH 7.5.**

Constants	Cerussite	Hydrocerussite	References
k_1*	20.0 ± 4.0 $M^{-1}·h^{-1}$	30.0 ± 2.4 $M^{-1}·h^{-1}$	our study
k_2	(5.5 ± 1.1) $\times 10^5$ $M^{-2}·h^{-1}$	(7.5 ± 0.6) $\times 10^5$ $M^{-2}·h^{-1}$	our study
k_3	(6.0 ± 1.3) $\times 10^3$ $M^{-2}·h^{-1}$	(6.0 ± 1.0) $\times 10^3$ $M^{-2}·h^{-1}$	our study
k_4	(6.0 ± 1.2) $\times 10^3$ $M^{-2}·h^{-1}$	(4.0 ± 0.7) $\times 10^3$ $M^{-2}·h^{-1}$	our study
k_5	(3.0 ± 0.3) $\times 10^6$ $M^{-2}·h^{-1}$	(5.5 ± 0.6) $\times 10^6$ $M^{-2}·h^{-1}$	our study

564

565

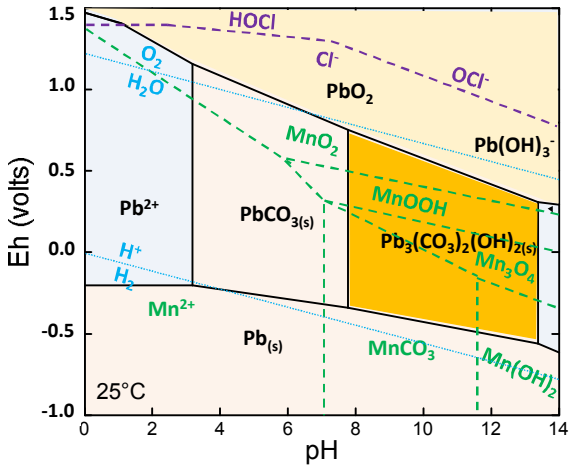

566

567 **Figure 1.** Eh-pH diagram of Pb-Mn-Cl at 25 °C and 1 bar total pressure. Predominance areas were
568 calculated for conditions with 2 mM Pb, 0.1 mM Mn, and 0.2 mM inorganic carbon. Boundaries
569 of predominance areas are shown for chlorine (purple), lead (black), and manganese (green)
570 species. Blue lines indicate the stability limits of water.

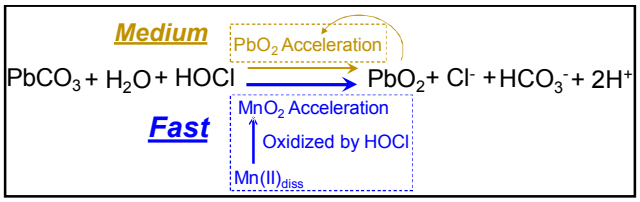

571

572 **Figure 2.** Conceptual model of PbO_2 formation from cerussite considering PbO_2 autocatalytic and

573 MnO_2 catalytic effects. Both the hypochlorite ion and hypochlorous acid can oxidize Pb(II) to

574 Pb(IV), and only the hypochlorite ion is shown here for the sake of simplicity.

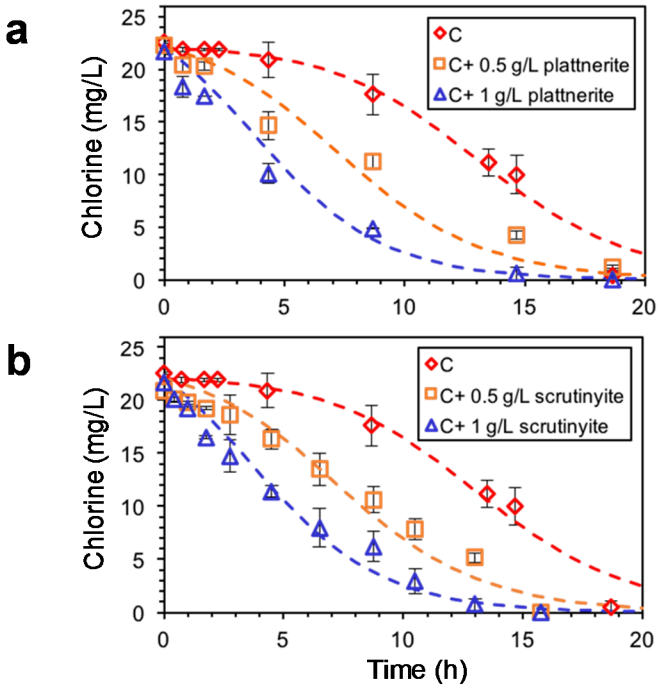

575

576 **Figure 3.** Oxidation of cerussite (C) by chlorine with and without (a) plattnerite and (b) scrutinyite.
577 Conditions: pH = 7.5 ± 0.2, initial free chlorine = 0.31 mM (22 mg/L as Cl_2), initial cerussite = 2
578 mM as Pb, DIC = 0.2 mM as C. Experimental results are shown as points and modeling results are
579 shown as dashed lines. The average values from duplicate experiments are shown, and the error
580 bars represent the standard deviation from the duplicate experiments.

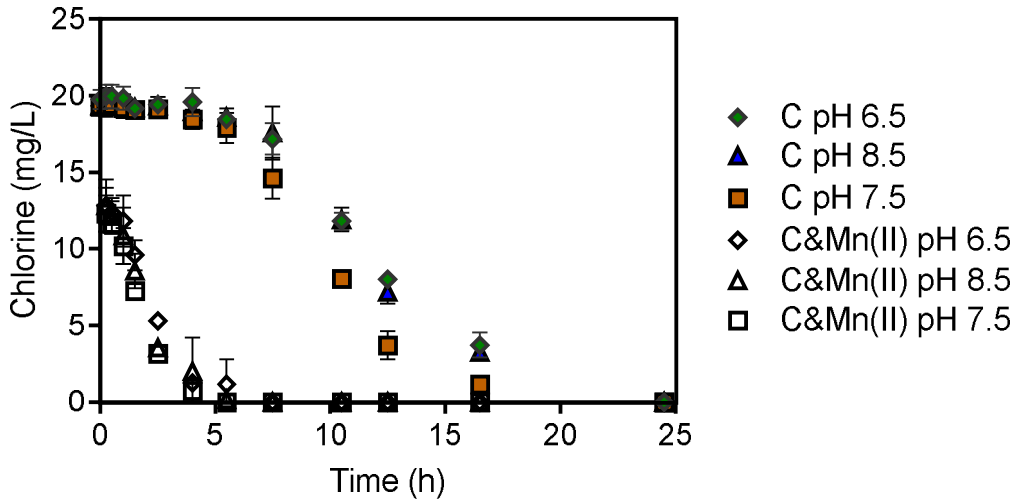

581

582 **Figure 4.** Effect of pH on cerussite oxidation. Condition: initial free chlorine = 0.31 mM (22 mg/L)

583 as Cl_2, initial Pb = 2mM, carbonate = 0.2 mM as C. Experimental results were shown as points.

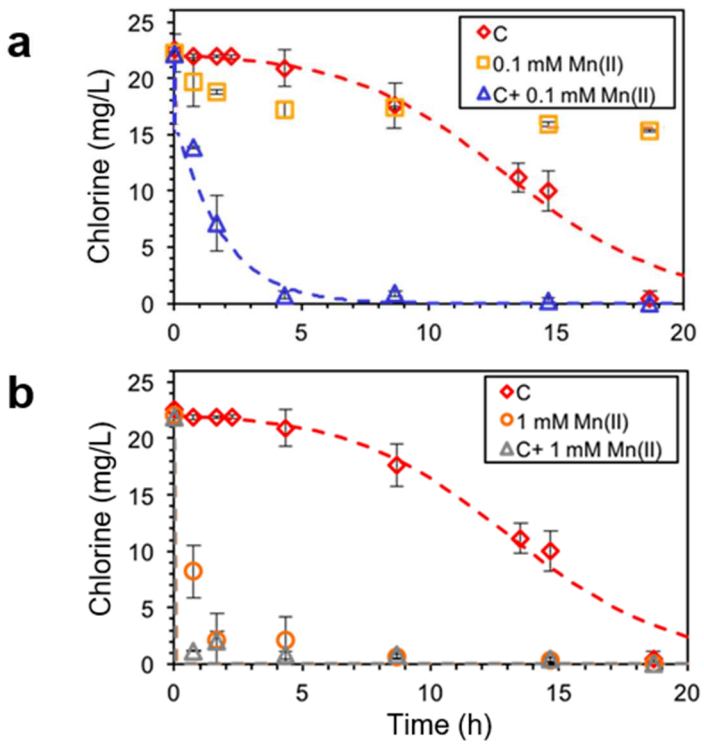

584

585 **Figure 5.** Oxidation of cerussite (C) by chlorine with (a) 0.1 and (b) 1 mM Mn(II) concentrations.
586 Conditions: pH = 7.5 ± 0.2, initial free chlorine = 0.31 mM (22 mg/L as Cl_2), initial Pb = 2 mM,
587 carbonate = 0.2 mM as C. Experimental results are shown as points and modeling results are shown
588 as dashed lines. The average values from duplicate experiments are shown, and the error bars
589 represent the standard deviation from the duplicate experiments.

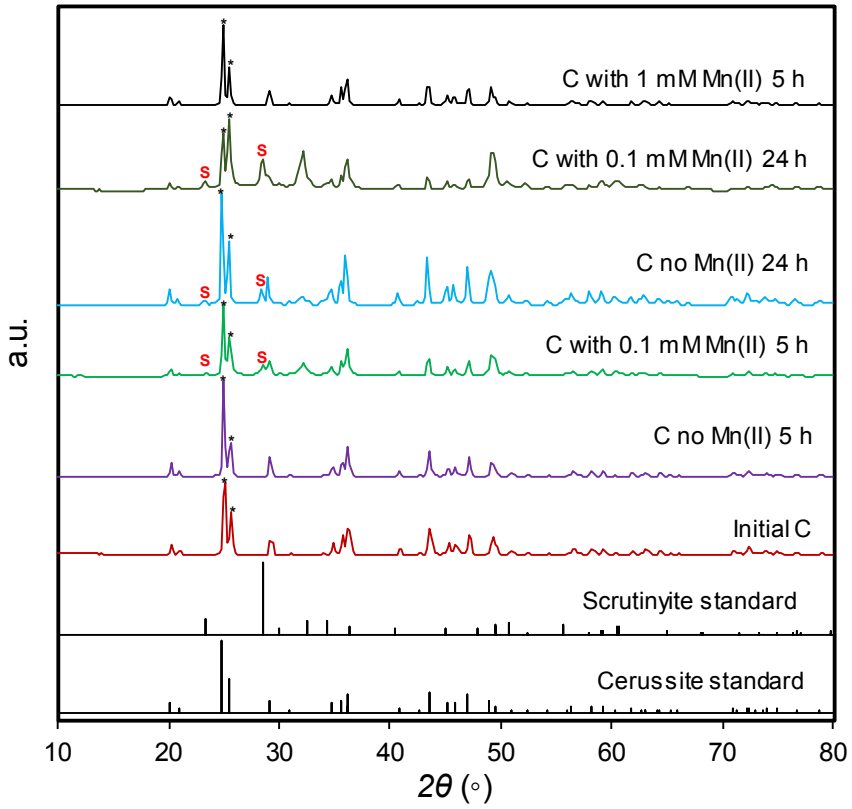

590

591 **Figure 6.** X-ray diffraction patterns of solids from cerussite (C) oxidation experiments. Dominant
592 peaks associated with scrutinyite and cerussite were indicated, and reference powder diffraction
593 file patterns are included for these phases (04-008-7674 and 01-073-4362). The main peaks of
594 scrutinyite are indicated as S. The main peaks of cerussite are indicated as *.

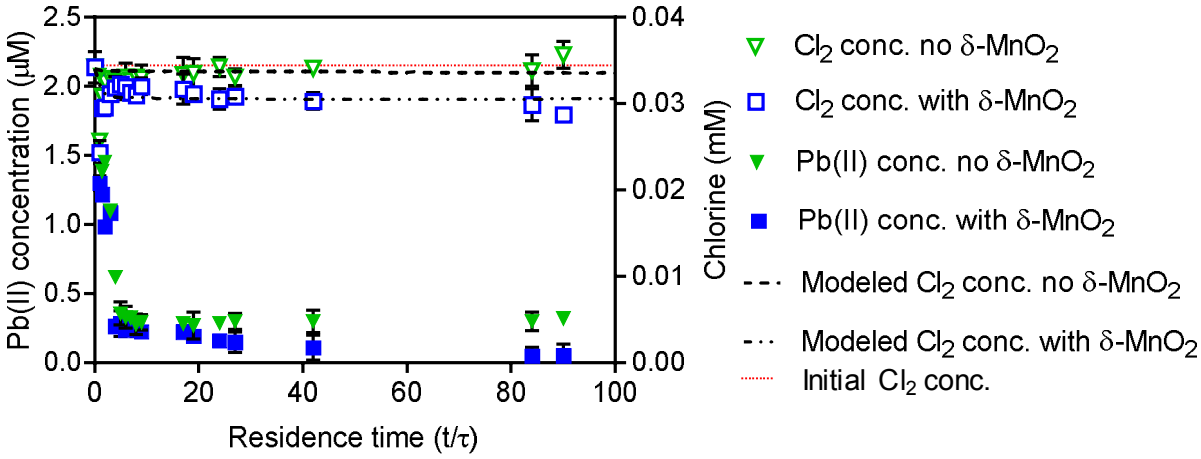

595

596 **Figure 7.** Effluent lead and chlorine concentrations from flow-through experiments with cerussite
597 in the absence and presence of δ-MnO_2. Experiments were conducted at a hydraulic residence time
598 of 20 minutes. Samples were not taken during the middle of the experiments (50 to 80 τ). Modeling
599 results are shown as dashed lines. Conditions: pH = 7.5 ± 0.2, initial free chlorine = 0.034 mM
600 (2.4 mg/L) as Cl_2, initial Pb = 2 mM, carbonate = 0.2 mM as C.